Lipid Reorganization Induced by Shiga Toxin Clustering on Planar Membranes

Barbara Windschiegl[1], Alexander Orth[1], Winfried Römer[2], Ludwig Berland[3], Bahne Stechmann[2], Patricia Bassereau[3], Ludger Johannes[2], Claudia Steinem[1]*

1 Institut für Organische und Biomolekulare Chemie, Georg-August Universität, Göttingen, Germany, 2 Institut Curie, Centre de Recherche, CNRS UMR 144, Laboratoire Trafic, Signalisation et Ciblage Intracellulaires, Paris, France, 3 Institut Curie, Centre de Recherche, CNRS UMR 168, Laboratoire Physico-Chimie, Paris, France

Abstract

The homopentameric B-subunit of bacterial protein Shiga toxin (STxB) binds to the glycolipid Gb_3 in plasma membranes, which is the initial step for entering cells by a clathrin-independent mechanism. It has been suggested that protein clustering and lipid reorganization determine toxin uptake into cells. Here, we elucidated the molecular requirements for STxB induced Gb_3 clustering and for the proposed lipid reorganization in planar membranes. The influence of binding site III of the B-subunit as well as the Gb_3 lipid structure was investigated by means of high resolution methods such as fluorescence and scanning force microscopy. STxB was found to form protein clusters on homogenous 1,2-dioleoyl-*sn*-glycero-3-phosphocholine (DOPC)/cholesterol/Gb_3 (65:30:5) bilayers. In contrast, membranes composed of DOPC/cholesterol/sphingomyelin/Gb_3 (40:35:20:5) phase separate into a liquid ordered and liquid disordered phase. Dependent on the fatty acid composition of Gb_3, STxB-Gb_3 complexes organize within the liquid ordered phase upon protein binding. Our findings suggest that STxB is capable of forming a new membrane phase that is characterized by lipid compaction. The significance of this finding is discussed in the context of Shiga toxin-induced formation of endocytic membrane invaginations.

Introduction

Shiga toxin (STx) produced by *Shigella dysenteriae* is a member of the so-called AB_5 class of bacterial toxins. STx consists of a hexameric assembly comprising a single catalytically active A-subunit possessing rRNA-specific *N*-glycosidase activity and a B-subunit (STxB), a pentamer of identical fragments, which is responsible for the toxin binding to the plasma membrane of the host cell [1]. This homopentameric STxB can bind up to 15 molecules of the plasma membrane-embedded neutral receptor globotriaosylceramide (Gb_3) [2,3] and allows the intracellular transport of the holotoxin and the delivery of the monomeric A-subunit into the cytosol leading to the inhibition of protein biosynthesis [4].

Once bound to the plasma membrane, it has been shown that STx can be internalized in a clathrin- and caveolae-independent process [5–8], and a recent study demonstrates that the lipids themselves contribute significantly to the earliest steps of toxin uptake into cells, that is, the formation of membrane invaginations [9]. These membrane invaginations appear to be concomitant with membrane reorganization, as deduced from experiments using the polarization sensitive membrane dye Laurdan on cells [9]. In particular, STxB binds with high apparent affinity to Gb_3 resulting in the formation of dynamic STxB clusters in a process that imposes negative curvature on the membrane [9,10]. Coarse grained membrane simulations have demonstrated that curvature-

mediated interactions can lead to protein clustering and the formation of invaginations [11]. In the case of STxB, the exact mechanism, by which local curvature is induced, still has not been described, even if it has been suggested, based on theoretical considerations that local lipid compaction might be the driving force [9].

Three different Gb_3 binding sites (I, II, and III) are found on each of the five B-fragments that constitute one homopentameric STxB subunit, and it is known that they contribute differently to the binding of STxB to cells. While a mutation in binding site I (D17E-STxB) decreases the binding affinity to cells by a factor of about three [12], a mutation in binding site III (W34A-STxB) does not. However, despite the same binding affinity, the latter mutant shows a strongly reduced binding capacity suggesting that binding site III serves as a recognition element for additional Gb_3 molecules after the protein has been bound [12]. The recruitment of Gb_3 molecules underneath STxB via binding site III may then result in the formation of Gb_3 clusters and membrane thickening as proposed by Ling et al. [3]. This, in turn, suggests that the molecular structure of Gb_3, i.e. the composition of the fatty acids, which determines the localization of the lipids in phase separated lipid bilayers [13,14] contributes considerably to Gb_3 cluster formation. By molecular modeling, Nyholm et al. [15] observed an influence of the fatty acid composition on the conformation and position of the Gb_3 head group at the membrane interface, which directly impacts the STxB binding affinity. This is further

corroborated by the finding that the binding affinity of STxB to bilayers composed of phosphatidylcholine (PC) and Gb$_3$ increases if the fatty acid chain length of PC decreases, which exposes the head group of Gb$_3$ more into the aqueous phase [16]. Of note, the binding affinity of STxB to Gb$_3$ was found to be larger if the receptor lipid was extracted from tissue, i.e. a mixture of Gb$_3$ molecules was presented, compared to neat synthetic Gb$_3$ molecules [17]. Furthermore, not only a higher binding affinity but also a larger binding capacity was found if a mixture of Gb$_3$ lipids varying in the fatty acid composition was used for STxB binding studies, when compared to single Gb$_3$ species [18]. These studies demonstrate a direct link between lipid structure and Shiga toxin interaction with cell membranes. The functional consequences of these differences have not yet been addressed directly.

In this study, we analyzed the molecular requirements for STxB-induced Gb$_3$ clustering and for the previously suggested lipid reorganization in planar membranes. The influence of binding site III of the protein as well as of the Gb$_3$ lipid structure on the lateral organization of STxB and the membrane was investigated by means of high resolution methods such as fluorescence and scanning force microscopy.

Results

Interaction of STxB with DOPC/cholesterol/Gb$_3$ bilayers

To investigate the formation of membrane invaginations induced by STxB binding, first a lipid mixture composed of 1,2-dioleoyl-sn-glycero-3-phosphocholine (DOPC) and cholesterol was chosen, doped with 5 mol% of purified porcine globotriaosylceramide (porcine Gb$_3$). The cholesterol content was adjusted to 30 mol% in accordance with its typical abundance in the plasma membrane of

eukaryotic animal cells. The specific binding of Cy3-labeled STxB to DOPC/cholesterol/porcine Gb$_3$ (65:30:5) giant unilamellar vesicles (GUVs, 10–30 μm in diameter) doped with 1 mol% Bodipy-PC at room temperature results in the formation of tubular membrane invaginations containing STxB (red fluorescence) and membrane components (green fluorescence) (Figure 1A) similar to what has been observed in experiments performed at 37°C [9].

To elucidate protein- and lipid reorganization processes with high lateral resolution upon STxB binding, we made use of fluorescence and scanning force microscopy (SFM) on planar solid supported membranes (SSMs). As membrane bending is constrained in SSMs, the observed protein distribution is not influenced by membrane deformation. The topography of planar membranes composed of DOPC/cholesterol/porcine Gb$_3$ (65:30:5) immobilized on atomically flat mica surfaces is featureless, i.e. no membrane domains are discernable (Figure S1), which is consistent with the homogeneous green Bodipy-PC fluorescence observed in GUVs (data not shown). In rare cases, small holes were identified as membrane defects confirming the formation of a bilayer on the surface. Binding of Cy3-labeled STxB results in a rather homogeneous fluorescence on the membrane, which is the result of high protein coverage of membrane bound STxB (Figure 2A). Only very rarely, black areas were found, which are assigned to membrane defects as proven by SFM (data not shown), while small white spots are attributed to larger protein aggregates attached to the surface. If the specific receptor Gb$_3$ is not present in the membrane, very week fluorescence was detected as a result of non-specific protein binding, mainly localized in membrane defects.

By means of SFM, the lateral organization of membrane-bound protein was visualized showing micrometer-sized, sometimes
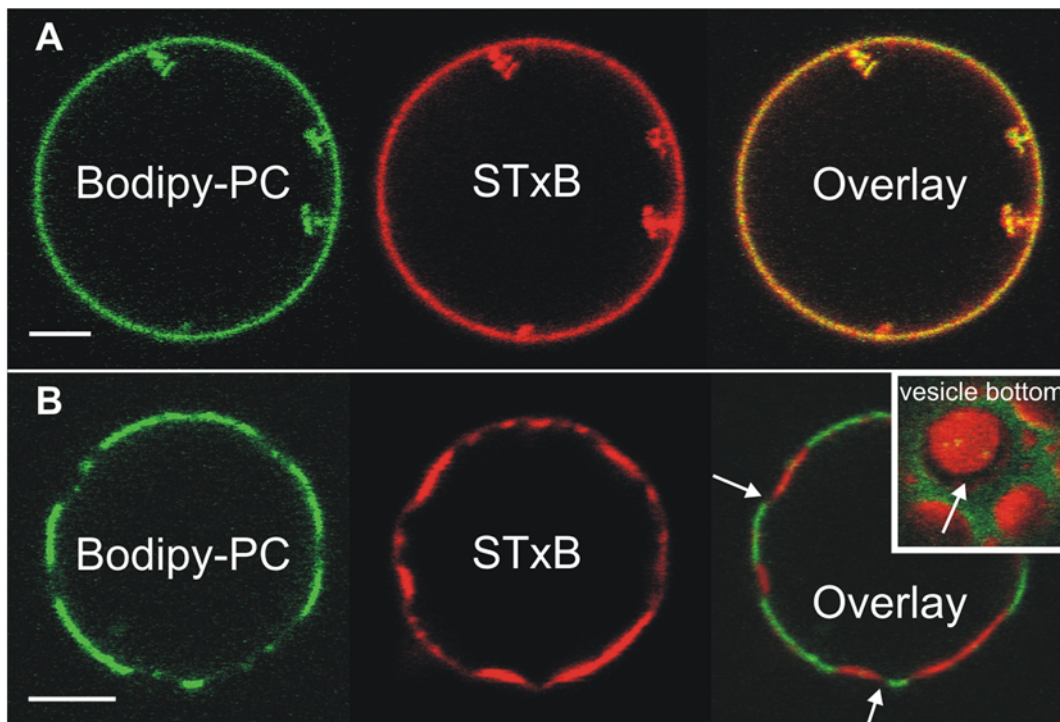
Figure 1. STxB binding to GUVs. (A) GUVs are composed of DOPC/cholesterol/porcine Gb$_3$ (65:30:5) doped with 1 mol% Bodipy-PC. The formation of tubular membrane invaginations containing STxB (red) and membrane components (green) was observed. Scale bar: 5 μm. (B) GUVs are composed of DOPC/sphingomyelin/cholesterol/porcine Gb$_3$ (41:41:13:5) doped with 1 mol% Bodipy-PC. The protein (red) binds to already phase-separated GUV membranes (green). No tubule formation was observed but shallow invaginations. Scale bar: 5 μm.
doi:10.1371/journal.pone.0006238.g001
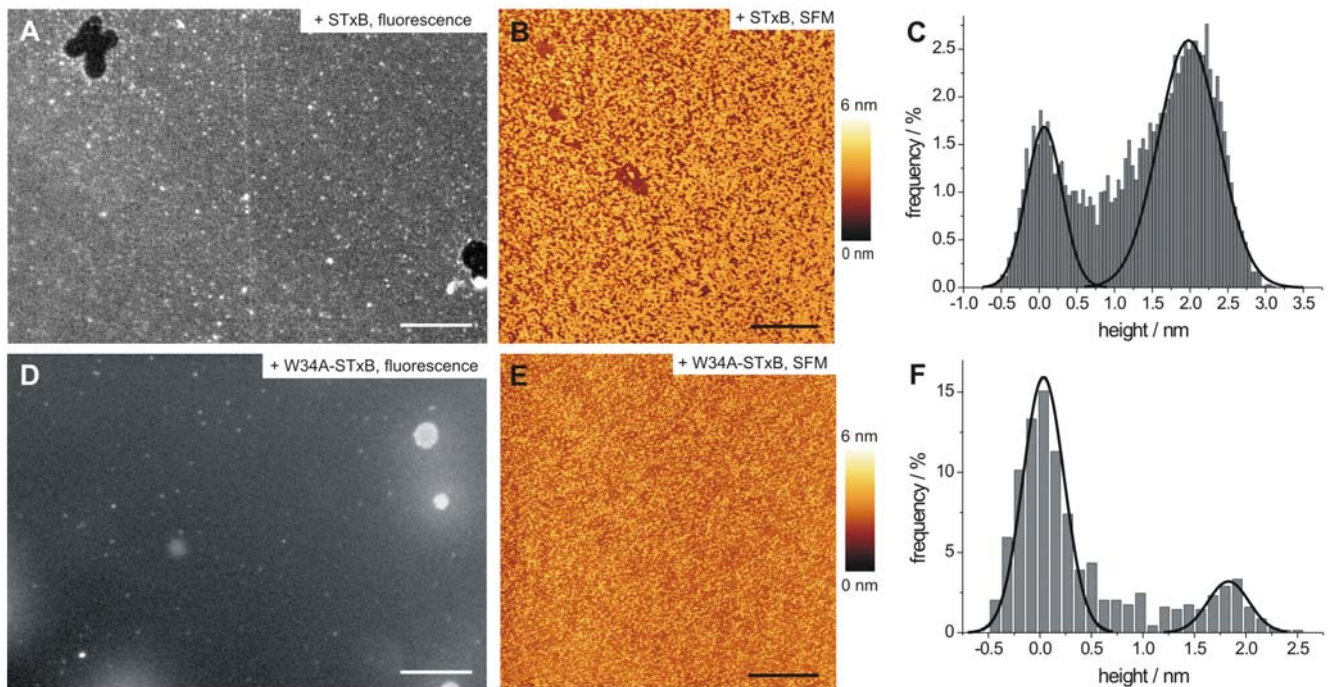
Figure 2. Binding of STxB to solid supported bilayers composed of DOPC/cholesterol/porcine Gb$_3$ (65:30:5). (A) Fluorescence image after Cy3-labeled STxB incubation. Scale bar: 15 μm. (B) SFM image after protein binding shows homogeneously distributed STxB clusters. Scale bar: 1 μm. (C) The height difference between protein-free and STxB covered membrane is (2.2±0.4) nm ($n = 35$). (D) Fluorescence micrograph after incubation with 60 nM Cy3-labeled W34A-STxB. Scale bar: 15 μm. (E) The SFM image shows homogeneously distributed protein clusters. Scale bar: 2 μm. (F) The height difference between protein-free and protein-covered membrane is (1.6±0.3) nm ($n = 12$).
doi:10.1371/journal.pone.0006238.g002

interconnected STxB clusters (Figure 2B). A detailed analysis of the protein clusters reveals an overall protein coverage of about 30–60%, while the height difference between membrane and protein turned out to be (2.2±0.4) nm ($n = 35$, Figure 2C).

To elucidate the influence of binding site III of STxB on the distribution of the protein on the membrane, the binding behavior of a STxB variant, in which the Gb$_3$ binding site III is inactivated by mutagenesis (W34A-STxB), was analyzed by fluorescence and scanning force microscopy. Even though the mutant protein still binds to membranes composed of DOPC/cholesterol/porcine Gb$_3$ (65:30:5) as demonstrated by fluorescence microscopy (Figure 2D), the overall protein cluster size appears to be smaller (Figure 2E). As the molecular dimensions of the mutant protein are identical to those of the wild-type protein, the height difference between membrane and protein was expected to be the same. In contrast to this prediction, we found that the height difference between membrane and protein was significantly smaller, as a value of (1.6±0.3) nm ($n = 12$) was determined (Figure 2F). These results demonstrate how the protein's Gb$_3$ binding capability modifies the overall membrane structure at STxB domains.

Interaction of STxB with DOPC/sphingomyelin/ cholesterol/Gb$_3$ bilayers

In contrast to the lipid mixture discussed in the previous section, GUV membranes composed of a lipid raft mixture, namely DOPC/sphingomyelin/cholesterol/porcine Gb$_3$ (41:41:13:5) doped with 1 mol% Bodipy-PC was used. These membranes are phase separated at room temperature as concluded from the observed inhomogeneous Bodipy-PC fluorescence (data not shown). The fluorophore is excluded from the liquid ordered (l_o-) phase, while it is well soluble in the liquid disordered (l_d-) phase

mainly composed of DOPC. The dark l_o-phase is largely enriched in sphingomyelin, and cholesterol [19–21]. Cy3-labeled STxB is found at the l_o-phase (Figure 1B) implying the preferential localization of porcine Gb$_3$ in the l_o-phase after protein binding. Interestingly, STxB fluorescence found at the border of the l_o- and l_d-phase is very faint, which might be a result of a preferential STxB clustering within the l_o-domains (Figure 1B, overlay, vesicle bottom). Tubule formation was, however, not observed with this lipid composition after protein binding but only shallow invaginations, even after vesicle deflation.

To elucidate this observation in more detail, planar bilayers composed of DOPC/sphingomyelin/cholesterol/porcine Gb$_3$ (40:35:20:5) were analyzed by SFM, also showing the coexistence of two lipid phases (Figure 3A). The lower phase is assigned to the l_d-phase enriched in DOPC, while the l_o-phase exhibits a membrane thickness, which is (0.7±0.2) nm ($n = 46$) larger than the l_d-phase as a result of a more ordered lipid packing of sphingomyelin, and cholesterol (Figure 3D), as reported previously [22–25].

Addition of Cy3-labeled STxB results in an inhomogeneous protein fluorescence (Figure 3B). A correlation of this fluorescence with SFM images allowed us to resolve the lateral protein distribution and membrane structure in more detail. Three different heights were found in the SFM topography image (Figure 3C). The lowermost structures are attributed to the l_d-phase and correspond to the dark areas in the fluorescence image with respect to form, distribution and number. As no protein fluorescence is emitted from those areas, it is concluded that STxB does not bind to the l_d-phase. The areas of bright protein fluorescence are a result of Cy3-labeled STxB bound to the liquid ordered phase (Figure 3B). By means of SFM imaging (Figure 3C) fractal STxB clusters bound to porcine Gb$_3$, which are located in
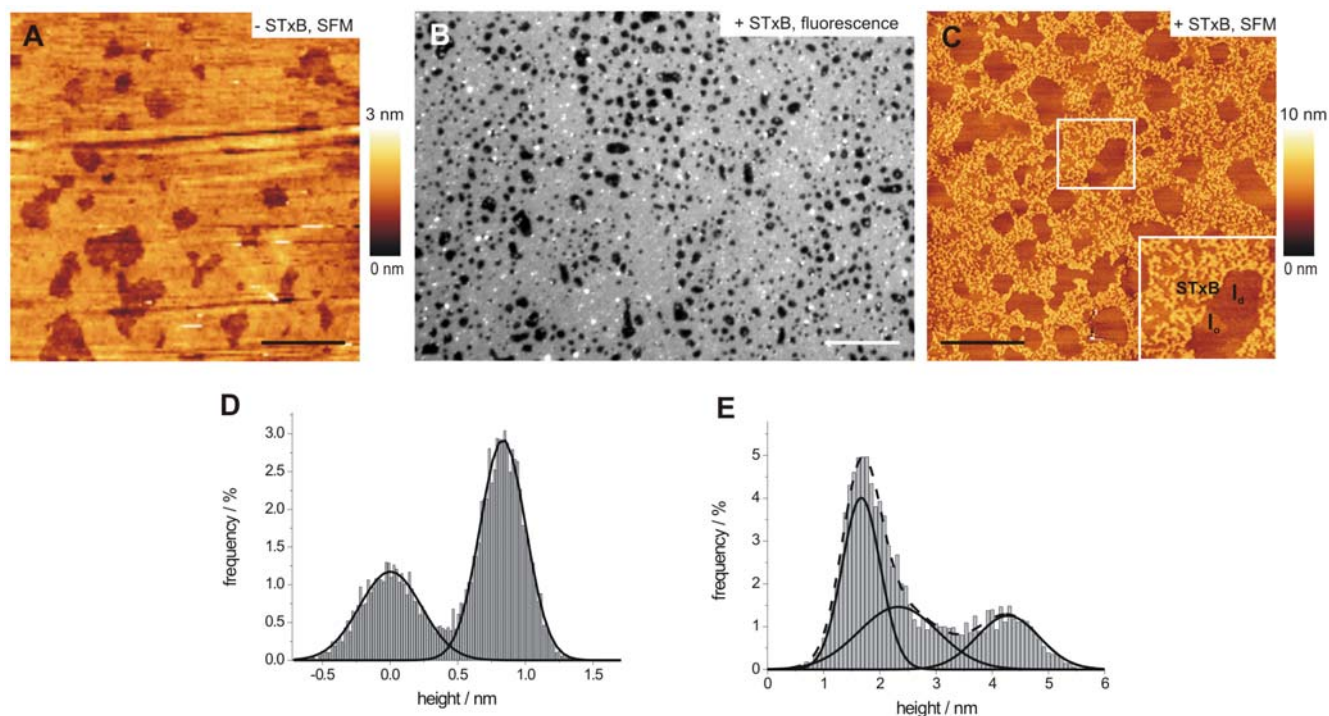
Figure 3. Binding of STxB to solid supported bilayers composed of DOPC/sphingomyelin/cholesterol/porcine Gb$_3$ (40:35:20:5). (A) In the absence of STxB the topographic SFM image of the bilayer shows the coexistence of a l_o- and l_d-phase. Scale bar: 5 μm. (B) Fluorescence micrograph after Cy3-labeled STxB incubation. Scale bar: 15 μm. (C) The SFM image shows STxB clusters located at the l_o-phase. Scale bar: 5 μm. (D) Statistical height analysis reveals the l_o-phase to be (0.7±0.2) nm ($n = 46$) higher than the l_d-phase. (E) The height difference between STxB and the l_o-phase exhibits (2.2±0.2) nm ($n = 26$) (typical histograms are shown, respectively).
doi:10.1371/journal.pone.0006238.g003

the l_o-phase, became discernable. Only small areas in the l_o-phase can be identified, on which no protein has been bound to, which might be explained by a local depletion of the receptor lipid Gb$_3$. The height difference between the lowermost (l_d-phase) and the observed medium height level (l_o-phase without protein) was determined by line analysis, confirming the expected height difference of 0.6 nm between l_d- and l_o-phase prior to protein addition [22–25]. We could not observe any preferential binding of the protein to the interface region of l_o- and l_d-phase, which makes a clear distinction of these areas possible. From areas, where only the l_o-phase and the protein submonolayer were present, we determined the height difference between adsorbed STxB and the l_o-phase rather accurately to a value of (2.2±0.2) nm ($n = 26$) by histogram analysis (Figure S2). A histogram of an area that contains all three different heights (l_o-phase, l_d-phase, and protein layer) reproduces the obtained height differences, but it is more difficult to unambiguously separate them (Figure 3E).

Lipid reorganization in planar bilayers by STxB binding

It is assumed that STxB binding to the l_o-phase of DOPC/sphingomyelin/cholesterol/porcine Gb$_3$ (40:35:20:5) membranes results in lipid reorganization. To prove this hypothesis, planar membranes were labeled with two different fluorescent lipids. 0.1 mol% of DOPC were replaced by TexasRed DHPE, which is preferentially localized in the l_d-phase, while further 0.2 mol% DOPC were substituted by perylene. Figure 4A/C (green color) show perylene fluorescence images prior to the addition of STxB. Large fluorescently labeled areas are discernable, with dark domains in between, where the perylene fluorophore is excluded. The black areas in the perylene fluorescence appear bright in the TexasRed DHPE fluorescence images (Figure 4B/C, red color)

confirming that the perylene fluorophore is mainly localized in the l_o-phase. Small white spots are assigned to residual vesicles adsorbed on the bilayer.

After protein incubation, the appearance of the fluorescence images has changed considerably. Rather circular domains up to 10 μm in diameter are visible in the TexasRed DHPE fluorescence (Figure 4E/F, red color) assigning the l_d-phase. To quantify this, the circularity of the l_d-domains was determined, which increases from 0.66±0.21 to 0.81±0.17 after protein binding. The same circularity of the l_d-domains (0.83±0.15) was found by analyzing the Cy3-fluorescence image after STxB binding (Figure 3B). Of note, also the perylene fluorophore is now preferentially located in the l_d-phase (Figure 4D/F, green color) indicating that the partition of the perylene fluorophore between the l_o- and l_d-phase has changed upon STxB binding. This observation is further supported by an overlay image showing both, the fluorescence of Cy3-labeled STxB and perylene, which demonstrates that the protein is localized at the l_o-phase, from which the perylene fluorophore is excluded (Figure 5A). We suggest that a tighter packing of the lipids in the l_o-phase, as a result of the formation of STxB-Gb$_3$ complexes, leads to the exclusion of the perylene fluorophore from this lipid phase. This tighter lipid packing in the l_o-phase is also reflected in the fraction area of l_o-phase in the bilayer, which decreases from 72% prior to protein binding to 63% after protein adsorption as determined by pixel analysis of the fluorescence images (see Figure 4B/E). Furthermore, SFM images (Figure 4C/F, insets) reveal that, after STxB has been bound, small l_o-domains appear within the l_d-domains, which could not be resolved by fluorescence microscopy.

As Gb$_3$ appears to be the major player for lipid reorganization and compaction, we further elucidated the impact of the packing
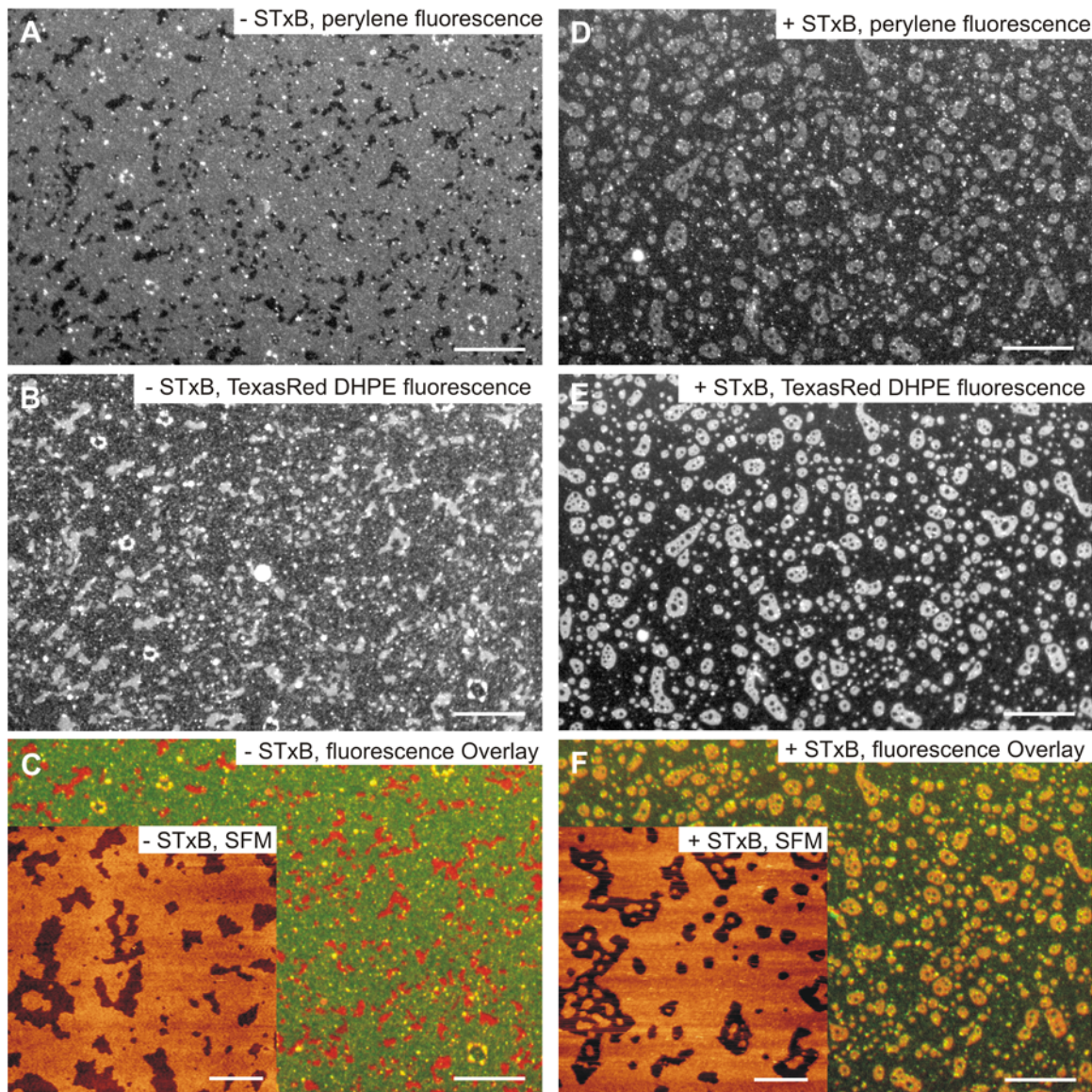
Figure 4. Fluorescence and scanning force micrographs of solid supported bilayers composed of DOPC/sphingomyelin/cholesterol/ porcine Gb$_3$ (40:35:20:5). (A, B, C) Fluorescence images prior to the addition of STxB. (A) 0.2 mol% perylene replaces DOPC and its fluorescence visualizes the l_o-phase. Scale bar: 20 μm. (B) The l_d-phase of the same area was detected with the fluorophore TexasRed DHPE (0.1 mol%). Scale bar: 20 μm. (C) Overlay of the fluorescence images shown in (A) and (B) together with the corresponding SFM image (inset). The images are false colored with the TexasRed DHPE fluorescence in red and the perylene fluorescence in green. Scale bar: 20 μm. (D, E, F) Fluorescence images after incubation of the membrane with 60 nM STxB. (D) The fluorophore perylene is enriched in the l_d-phase. Scale bar: 20 μm. (E) The fluorophore TexasRed DHPE is found in the same lipid phase, the l_d-phase. Scale bar: 20 μm. (F) Overlay of the fluorescence images shown in (D) and (E). The SFM image shows small l_o-domains within the l_d-domains (F, inset). Scale bar: 20 μm.
doi:10.1371/journal.pone.0006238.g004

parameter of Gb$_3$ on the redistribution of perylene, which indicates lipid compaction, by defining and varying its bound fatty acid side chain (Gb$_3$ (22:0) and Gb$_3$ (22:1[13])). Compared to membranes doped with porcine Gb$_3$ (Figure 5A), the protein appears rather homogeneously distributed on Gb$_3$ (22:1[13]) doped bilayers (Figure 5B), while an unambiguous separation of perylene and Cy3-labeled protein fluorescence is observed for Gb$_3$ (22:0) (Figure 5C) containing membranes. These results obtained on phase-separated planar supported membranes demonstrate the strong influence of the fatty acid side chain on the protein distribution and on cluster formation.

STxB binding to lipid monolayer systems

By using planar lipid monolayers at the air/water interface, a versatile system is available, which enabled us to monitor changes in membrane domains and the formation of lipid phases at a defined surface pressure. A lipid mixture composed of DOPC doped with 1 mol% Bodipy-PC/sphingomyelin/cholesterol/porcine Gb$_3$ (40:35:20:5) was spread on a PBS buffered subphase, the monolayer compressed to a surface pressure of 30 mN m^{-1} (Figure S3) and the phase behavior analyzed by fluorescence microscopy. At 30 mN m^{-1}, coexistence of two lipid phases was observed. Round as well as elongated domains were discernable,
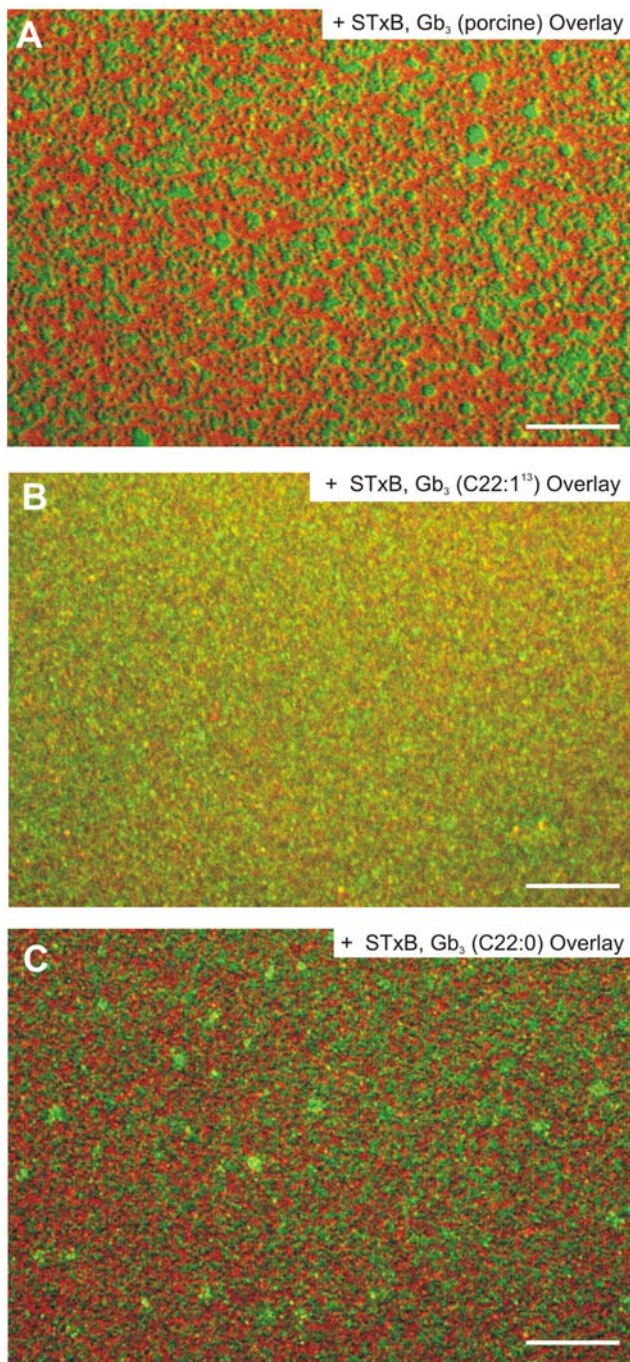
Figure 5. Overlay of fluorescence images of DOPC/sphingo-myelin/cholesterol/Gb$_3$ (40:35:20:5) planar bilayers after STxB binding. The Cy3-labeled STxB is shown in red, the perylene fluorescence in green. (A) Porcine Gb$_3$. Scale bar: 15 µm. (B) Gb$_3$ (22:1[13]). Scale bar: 15 µm. (C) Gb$_3$ (22:0). Scale bar: 15 µm.
doi:10.1371/journal.pone.0006238.g005

which are assigned to the l_o-phase enriched in sphingomyelin, and cholesterol (Figure 6A) [26,27]. Bodipy-PC is localized in the surrounding l_d-phase mostly composed of DOPC. Cy3-labeled STxB was injected into the subphase, which enabled us to monitor the Bodipy-PC and Cy3-fluorescence quasi-simultaneously after the protein had been bound to the monolayer. After protein binding, the Bodipy-PC fluorescence images show rather irregu-larly shaped dark l_o-phase domains, which appear bright in the

Cy3-fluorescence indicating that the protein is solely adsorbed on the l_o-phase domains (Figure 6C). A detailed pixel analysis of the Bodipy-PC fluorescence images reveals that the overall area occupied by l_o-phase does not change considerably upon protein binding. However, 30 minutes after protein addition, the number of l_o-phase domains per monolayer area has increased from (330 ± 70) mm^{-2} to (750 ± 290) mm^{-2}, which is primarily a result of an increase in the number of small domains (<1000 µm^2) from 72% to 94% of all l_o-phase domains. This result suggests that STxB binding to the monolayer induces new l_o-phase domains similar to what has been observed in bilayers (compare Figure 4C/F, insets).

Surprisingly, darker areas become discernable within the larger l_o-phase domains (Figure 6B) after protein binding. The slight change in fluorescence intensity can be more easily visualized by the intensity profile depicted in Figure 6D. This finding implies lipid compaction within the existing l_o-phase, leading to a strong exclusion of the Bodipy-PC fluorophore.

The same experiment was performed using the mutant W34A-STxB lacking binding site III. While Cy3-labeled protein binding to the l_o-phase was observed (Figure 7A), the total number of domains per monolayer area decreased from (430 ± 140) mm^{-2} prior protein addition to (320 ± 120) mm^{-2} 30 minutes after STxB binding. Moreover, darker areas within the l_o-phase were not found (Figure 7B).

To elucidate whether STxB is indeed capable of inducing new membrane domains, we started from a non-phase separated lipid monolayer and investigated, whether dark domains are induced upon binding of STxB. A monolayer composed of DOPC doped with 1 mol% Bodipy-PC/sphingomyelin/cholesterol/porcine Gb$_3$ (65:10:20:5) was spread at the air/water interface (Figure S3). Before protein binding, the monolayer does not show phase separation at a surface pressure of 10–35 mN m^{-1} as deduced from fluorescence images (Figure 8A). However, after STxB binding, dark domains with a dendritic shape become discernable in the Bodipy-PC fluorescence images (Figure 8B), which appear bright in the Cy3-fluorescence images demonstrating that the protein has been bound to these newly formed irregularly shaped liquid ordered domains (Figure 8C). These findings suggest that the protein is capable of forming l_o-phase domains probably enriched in Gb$_3$. The same experiment was performed with the mutant W34A-STxB and no formation of l_o-phase domains was observed (data not shown).

Discussion

Previously, it has been shown that Shiga toxin is able to form tubules and buds in cellular and artificial systems, which was discussed in terms of protein-lipid nanodomain formation [9]. Such domains might be a direct result of protein binding leading to receptor clustering [28], which, in turn, can modulate the entire membrane organization. Here, we have shown that tubule formation in GUVs occurs not only at 37°C but also at room temperature, if a DOPC/cholesterol/porcine Gb$_3$ (65:30:5) lipid mixture is used. In contrast, only shallow deformations are formed in phase separated GUV membranes composed of DOPC/sphingomyelin/cholesterol/porcine Gb$_3$ (41:41:13:5) with an inhomogeneous Cy3-STxB fluorescence found at the border of the l_o- and l_d-phase suggesting STxB clustering within the l_o-domains. In GUV experiments addressing cholera toxin binding to G$_{M1}$ doped lipid bilayers, Baumgart et al. [20] were able to correlate the lipid domain composition and local membrane curvature proposing that these factors are important for membrane invagination processes.
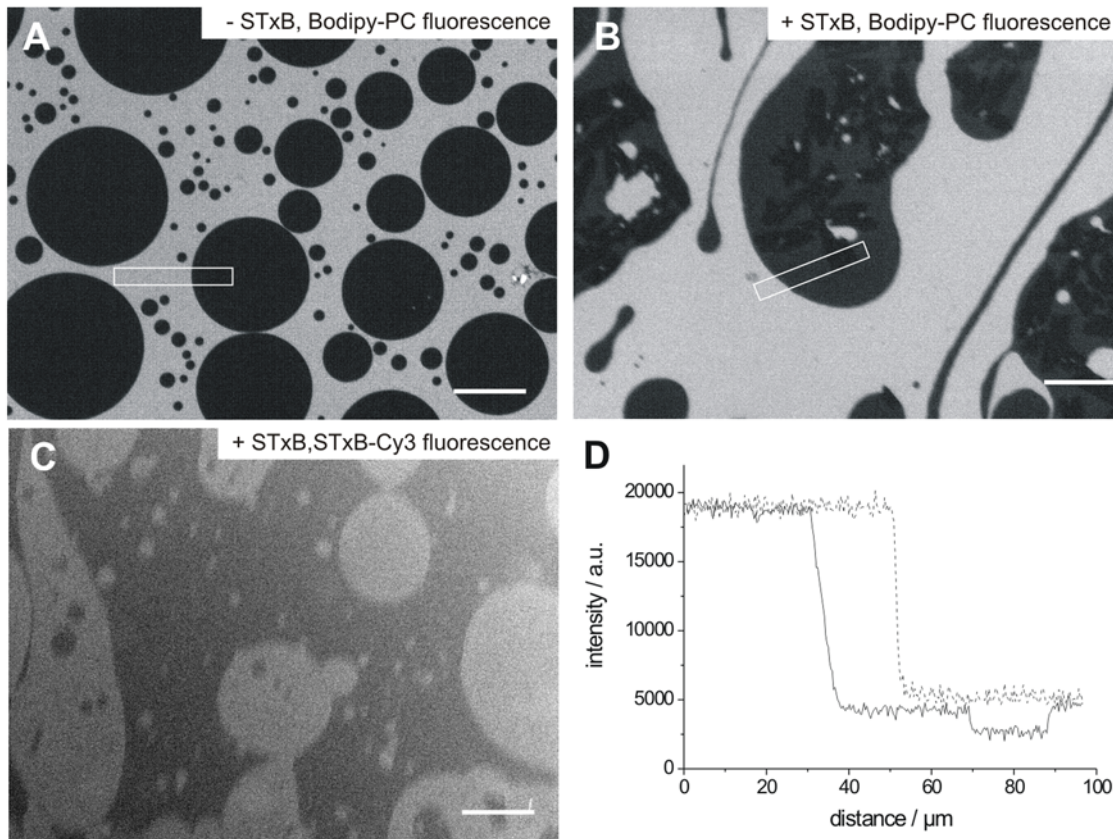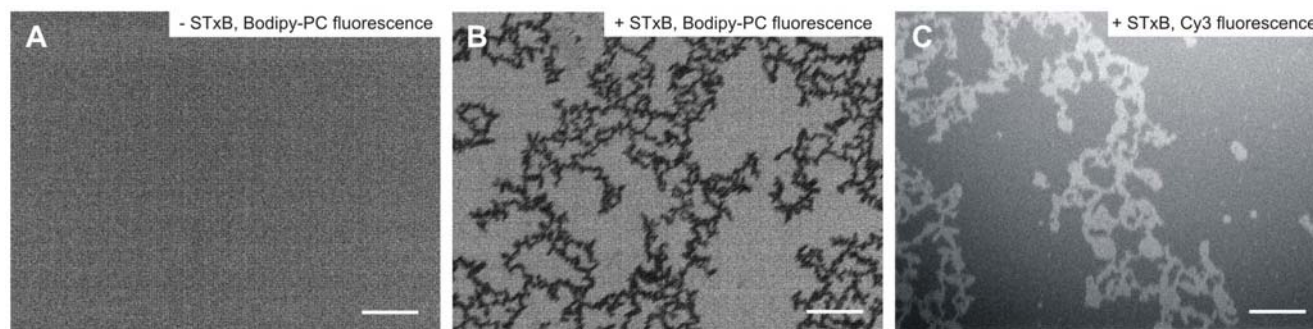
Figure 6. Fluorescence micrographs of lipid monolayers at the air/water interface. The monolayers are composed of DOPC doped with 1 mol% Bodipy-PC/sphingomyelin/cholesterol/porcine Gb$_3$ in a molar ratio of 40:35:20:5. (A) Without bound protein, round dark domains were observed at a surface pressure of 30 mN m^{-1}, which are assigned to the l_o-phase. Scale bar: 50 μm. (B) Bodipy-PC fluorescence after injecting 60 nM Cy3-labeled STxB into the PBS buffered subphase. Scale bar: 50 μm. (C) Cy3-STxB fluorescence after the addition of protein. Scale bar: 50 μm. (D) Average profiles of 40 line scans of the fluorescence intensity obtained in the white rectangles shown in Figure (A) (dotted line) and (B) (solid line).
doi:10.1371/journal.pone.0006238.g006

Here, the combination of fluorescence and scanning force microscopy on membranes immobilized on solid substrates enabled us to investigate the organization of membrane bound STxB and elucidate the protein-induced reorganization of lipids within membranes. SFM images of STxB bound to DOPC/cholesterol/porcine Gb$_3$ (65:30:5) and DOPC/sphingomyelin/ cholesterol/porcine Gb$_3$ (40:35:20:5) bilayers revealed clustering of the protein similar to what has been observed for the lateral organization of cholera toxin bound to DOPC membranes containing G$_{M1}$ [29]. Surprisingly, we found a mean height of the protein clusters of 2.2 nm, even though the protein height as deduced from the crystal structure of STxB is expected to be only
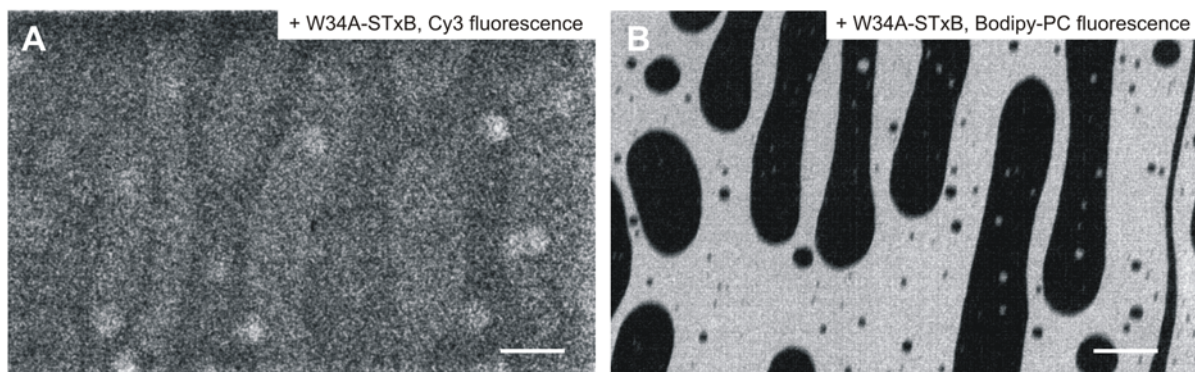
Figure 7. Fluorescence micrographs of lipid monolayers at the air/water interface. The monolayers are composed of DOPC/ sphingomyelin/cholesterol/Gb$_3$ in a molar ratio of 40:35:20:5 doped with 1 mol% Bodipy-PC at a surface pressure of around 30 mN m^{-1}. (A) Cy3-fluorescence image indicating binding of Cy3-labeled W34A-STxB to the l_o-phase domains. Scale bar: 50 μm. (B) Corresponding Bodipy-PC fluorescence. Scale bar: 50 μm.
doi:10.1371/journal.pone.0006238.g007

Figure 8. Fluorescence micrographs of lipid monolayers at the air/water interface. The monolayers are composed of DOPC doped with 1 mol% Bodipy-PC/sphingomyelin/cholesterol/porcine Gb_3 in a molar ratio of 65:10:20:5 at surface pressures between 25–30 mN m^{-1}. (A) Bodipy-PC fluorescence image prior STxB addition. Scale bar: 50 μm. (B) After STxB addition small dark, ordered domains are formed. Scale bar: 50 μm. (C) Dark domains in the Bodipy-PC fluorescence appear bright in the Cy3-fluorescence. Scale bar: 50 μm.
doi:10.1371/journal.pone.0006238.g008

2 nm [30,31]. In general, protein heights determined by SFM are often under-estimated [32] because of the force applied by the tip and a non-perfect protein packing. Indeed, membrane bound W34A-STxB with the same molecular dimensions, but only two Gb_3 binding sites per monomer, exhibits a smaller height of 1.6 nm compared to that of the crystal structure as expected. Hence, we conclude that the observed 28% height increase of the protein domains compared to those of W34A-STxB is a result of membrane thickening induced by the accumulation of Gb_3 owing to the occupation of binding site III of each STxB subunit after protein binding as proposed by Bast et al. [12] and Ling et al. [3]. A higher lipid packing density, as suggested by the perylene redistribution experiments (see below) in DOPC/sphingomyelin/cholesterol/Gb_3 (40:35:20:5) membranes (Figure 4 and 5) might also contribute to this bilayer thickening. This composition phase separates forming a l_o- and l_d-phase, which is in good agreement with reported ternary phase diagrams of DOPC, cholesterol and sphingomyelin [33]. STxB solely binds to Gb_3 and is excluded from the l_d-phase. Hence, it can be concluded that Gb_3 is located within the l_o-phase after STxB has been bound. For G_{M1}, it has been reported that it is localized in the l_o-phase of lipid monolayers composed of phosphatidylcholine, sphingomyelin and cholesterol [27,34].

Besides protein clustering, an unexpected observation is that STxB binding to a DOPC/sphingomyelin/cholesterol/Gb_3 (40:35:20:5) lipid mixture results in a redistribution of the fluorophore perylene from the l_o- in the l_d-phase. In GUV experiments, perylene was preferentially found in l_o-phases in ternary lipid mixtures containing *egg* sphingomyelin, DOPC and cholesterol [20]. However, Baumgart et al. [35] reported that perylene does not show any favored localization in ternary mixtures containing *brain* sphingomyelin. Even though we used *brain* sphingomyelin, perylene is unambiguously localized in the l_o-phase in solid supported membranes composed of sphingomyelin, DOPC and cholesterol before the addition of protein. After protein binding, the fluorophore is colocalized with TexasRed DHPE in the l_d-phase. Following the idea that the protein generates a new membrane organization comprising STxB-Gb_3 complexes that are tightly packed, the fluorophore is excluded from this further compressed membrane phase and thus partitions into the l_d-phase. This notion is in agreement with the increased height difference observed in the topography images shown in Figure 2 and 3 and the fact that the total area occupied by l_o-phase is reduced by 10% upon protein binding. In addition, the circularity of the l_o-domains increases after protein addition, which

might be a result of an increased line tension owing to the increased height difference between the l_o-domains and the surrounding l_d-phase membrane. Recently, Garcia-Sáez et al. [36] also showed that an increase in line tension induced by a hydrophobic mismatch in solid supported membranes leads to an increase in circularity of the membrane domains. We thus conclude that a lipid compaction in the l_o-phase occurs, which is induced by the bound protein. We suggest that Gb_3 lipids compact upon STxB binding, leading to lipid reorganization within the membrane and eventually results in the formation of an additional membrane phase enriched in Gb_3 and STxB. Even though the lipid organization and the composition of this new phase is not yet fully understood, it is well conceivable that the packing parameter of Gb_3 might influence this lipid compaction and reorganization process, which was corroborated by fluorescence overlay experiments. Initially phase separated planar membranes containing Gb_3 with a long chain saturated fatty acid (22:0) demix in the presence of STxB similarly to what has been observed for membranes containing porcine Gb_3, which is composed of 70% saturated and 30% unsaturated fatty acids. In contrast, STxB is rather homogeneously bound to membranes containing Gb_3 with a mono-unsaturated fatty acid (22:1^{13}), which is less densely packed, and is not organized in macroscopic domains, from which perylene is excluded.

The proposed lipid compaction was further supported by monolayer experiments at the air/water interface, demonstrating that new l_o-phase domains are formed upon STxB binding and a denser lipid packing is induced within already existing liquid ordered phase domains. That the mutant W34A-STxB does not influence the phase behavior of the monolayer further suggests that Gb_3 clustering underneath STxB is presumably a prerequisite for the formation of l_o-phase domains.

Based on our current knowledge, we propose a model for protein binding and lipid reorganization as depicted in Figure 9. First, STxB binds via the high affinity binding sites I and II to Gb_3 and forms protein clusters. Via binding site III, more Gb_3 molecules are recruited underneath the protein, which results in membrane thickening and a close packing of the lipids. As a result of the increased line tension (red arrows) the membrane domains become more circular (A) and fuse to larger domains (B) in case of planar supported membranes [9,37,38]. In case of free membranes, such lipid reorganization and compaction generated by Gb_3 clustering can result either in large membrane domains with the formation of only small buds (see Figure 1B) or, if no large phase separation occurs, it leads to bending of the membrane (C) if
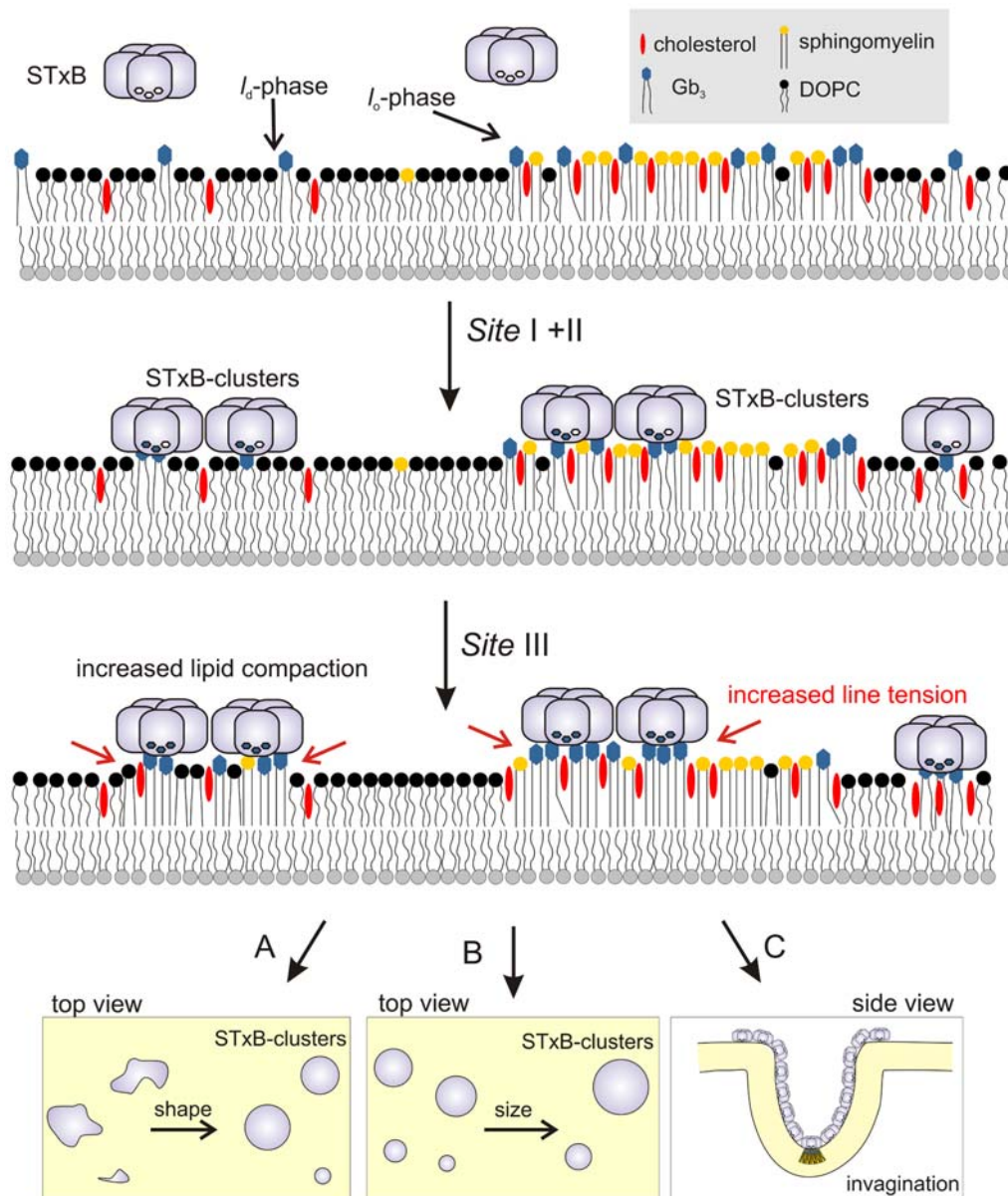
Figure 9. Model of the binding modes of STxB to Gb$_3$ containing membranes. The organization of the lipids in the bottom leaflet of the bilayer is not given in detail. For further details see text.

doi:10.1371/journal.pone.0006238.g009

the membrane tension is low enough (see Figure 1A). In conclusion, the presented results provide evidence for the STxB-induced formation of tightly packed membrane domains, whose intrinsic properties such as height mismatch and trans-bilayer stress may contribute to the driving forces required for the clathrin-independent plasma membrane invaginations in cells.

Materials and Methods

Materials

1,2-Dioleoyl-*sn*-glycero-3-phosphocholine (DOPC) was purchased from Avanti Polar Lipids (Alabaster, AL, USA); sphingomyelin, cholesterol, and the fluorescently labeled lipids Sulforhodamine 101 DHPE (TexasRed DHPE) and perylene were from Sigma-Aldrich (Taufkirchen, Germany); porcine globotriaosylceramide (Gb$_3$) was from Matreya (Pleasant Gap, PA, USA), Gb$_3$

(22:0) and Gb$_3$ (22:1[13]) was synthesized according to the procedure described previously (9). β-BODIPY 500/510 C$_{12}$-HPC (Bodipy-PC) was obtained from Molecular Probes (Eugene, OR, USA). Recombinantly expressed STxB and W34A-STxB as well as the modified Cy3-labeled STxB was purified as previously described [39]. All protein concentrations are referred to the molar mass of the STxB pentamer. Cantilevers (Ultrasharp CSC38) were purchased from Mikromasch (Tallinn, Estonia). Ultra-pure water (specific resistance of 18.2 MΩ/cm) was used, obtained from a Milli-Q purification system (Millipore, Billerica, MA) consisting of a Milli-RO3 plus and a Milli-Q plus 185 ion exchanger.

Giant unilamellar vesicles

GUVs were prepared by the electroformation technique as previously described [9,40]. Lipids were dissolved in the appropriate ratio in chloroform at a total concentration of

0.5 mg ml^{-1}. GUVs with a typical diameter of 10–30 μm were grown in a sucrose solution adjusted to 300 mOsm. They were transferred into a chamber containing Cy3-labeled STxB (200 nM) in PBS buffer.

Solid supported bilayers

Bilayers were prepared on mica surfaces by means of vesicle spreading. Stock solutions of DOPC, sphingomyelin, cholesterol, TexasRed DHPE, and Bodipy-PC, respectively were prepared in chloroform, while Gb$_3$ was dissolved in chloroform/methanol (2:1). Lipid films were formed at the bottom of glass test tubes under a stream of nitrogen at $T = 55°C$, desiccated under vacuum at 55°C for 3 h and stored at 4°C. Multilamellar vesicles (MLVs) were obtained by allowing the lipid films to swell in buffer solution (20 mM TRIS/HCl, 100 mM NaCl, 1 mM CaCl$_2$, pH 7.4) for 20 min at 55°C followed by vortexing three times for 30 sec every 5 min (total lipid concentration: 0.3 mg ml^{-1}). MLVs were subsequently converted into large unilamellar vesicles (LUVs) by extrusion using a mini extruder (LiposoFast, Avestin, Ottawa, Canada) supplied with a 50 nm polycarbonate membrane at 55°C. The LUVs were deposited on a freshly cleaved mica plate fixed in an open Teflon chamber with a lipid concentration of 0.3 mg ml^{-1} in the presence of 10 mM Ca^{2+}. After 1 h incubation at 55°C, the mica surface was rinsed with PBS buffer (1.5 mM KH$_2$PO$_4$, 8.1 mM Na$_2$HPO$_4$, 2.7 mM KCl, 136.9 mM NaCl, pH 7.4) at room temperature. Either Cy3-labeled or unlabeled STxB was added to the planar bilayer at room temperature. Non- and reversibly bound protein was removed after 1 hour by rinsing with PBS buffer.

Lipid monolayers at the air/water interface

STxB interaction with lipid monolayers at the air/water interface was investigated by means of a film balance equipped with a Wilhelmy system (Riegler & Kirstein, Potsdam, Germany). To reduce the volume of the subphase after monolayer compression, a small trough with a total volume of about 6 ml was placed into the Teflon trough of the film balance. Lipid mixtures dissolved in chloroform/methanol were spread onto a PBS buffered subphase and the lipid film was equilibrated for 15 min. After the monolayer was compressed with a velocity of 4.7 mm^2 s^{-1} to a surface pressure of 30 mN m^{-1}, the total subphase volume was reduced by delimiting the inserted small trough with two Teflon pieces and the film was equilibrated for another 15 min. STxB with a final concentration of 60 nM was injected into the subphase without disturbance of the monolayer via an inlet port of the small trough. The lateral organization of the lipid monolayer doped with 1 mol% Bodipy-PC and the localization of Cy3-labeled STxB was investigated by fluorescence microscopy, while the surface pressure was monitored simultaneously. All measurements were performed at $T = 20°C$.

Fluorescence microscopy

Fluorescence images of planar lipid monolayers and bilayers were obtained with an Axiotech Vario microscope (Carl Zeiss, Jena, Germany) equipped with an EC Epiplan-Neofluar 20×/0.5 objective (Zeiss) and filter set 44 (BP 475/40, FT 500, BP 530/50,

Zeiss) for monolayer inspection and a water immersion objective Achroplan 40×/0.8 W (Zeiss) for fluorescence analysis of solid supported bilayers. Filter set 45 (BP 560/40, FT585, BP 630/75, Zeiss) was used for Cy3-STxB and TexasRed DHPE fluorescence light detection and filter set 47 (BP 436/20, FT 455, BP 480/40, Zeiss) for perylene fluorescence.

Fluorescence images of GUVs were obtained at room temperature with a confocal microscope (LSM 510, Carl Zeiss, Jena, Germany) equipped with an oil immersion objective 63× PL APO HCX, 1.4 numerical aperture (Zeiss).

Scanning force microscopy

Surface images of solid supported bilayers were obtained in an open Teflon fluid chamber using a JPK NanoWizard II scanning force microscope (JPK Instruments, Berlin, Germany). Measurements were performed in PBS buffer in contact mode using microfabricated silicon tips with a typical resonance frequency of 10 kHz and a nominal spring constant of 0.03 N m^{-1}. Scan speed was adapted to the scan size and set between 0.6 and 2 Hz. Image resolution was 512×512 pixels. Height differences were extracted by pixel analysis of several SFM images with different image sizes.

Supporting Information

Figure S1 Solid supported bilayer composed of DOPC/cholesterol/porcine Gb$_3$ (65:30:5) in the absence of protein. The topographic SFM image of the bilayer shows no phase separation. Scale bar: 1 μm.
Found at: doi:10.1371/journal.pone.0006238.s001 (0.40 MB DOC)

Figure S2 Typical histogram of the height difference analysis between STxB and the l_o-phase of solid supported bilayers composed of DOPC/sphingomyelin/cholesterol/Gb$_3$ (40/35/20/5). The histogram was obtained from areas of the SFM images, where only STxB bound to the l_o-phase was found. The height was determined to (2.2 ± 0.2) nm ($n = 26$).
Found at: doi:10.1371/journal.pone.0006238.s002 (0.08 MB DOC)

Figure S3 A Compression isotherms of DOPC/sphingomyelin/cholesterol/porcine Gb$_3$ (40/35/20/5) with (red) and without (black) Bodipy-PC on a PBS-buffered subphase at 20°C. The area per molecule is given as an average value of the lipid mixture ($n = 5$), normalized to an $A_{20 \text{ mN/m}}$ value of 50 Å^2. B Compression isotherms of DOPC/sphingomyelin/cholesterol/porcine Gb$_3$ (65/10/20/5) with (red) and without (black) Bodipy-PC on a PBS-buffered subphase at 20°C. The area per molecule is given as an average value of the lipid mixture ($n = 5$), normalized to an $A_{20 \text{ mN/m}}$ value of 56 Å^2. For both mixtures, DOPC was replaced by Bodipy-PC.
Found at: doi:10.1371/journal.pone.0006238.s003 (0.57 MB DOC)

Author Contributions

References

1. Lacy DB, Stevens R (1998) Unraveling the structures and modes of action of bacterial toxins. Curr Opin Struct Biol 8: 778–784.
2. Pina DG, Johannes L, Castanho MARB (2007) Shiga toxin B-subunit sequential binding to its natural receptor in lipid membranes. Biochim Biophys Acta 1768: 628–636.
3. Ling H, Boodhoo A, Hazes B, Cummings MD, Armstrong GD, et al. (1998) Structure of the shiga-like toxin I B-pentamer complexed with an analogue of its receptor Gb$_3$. Biochemistry 37: 1777–1788.
4. Smith DC, Lord JM, Roberts LM, Johannes L (2004) Glycosphingolipids as toxin receptors. Sem Cell Develop Biol 15: 397–408.

5. Lauvrak SU, Torgersen ML, Sandvig K (2004) Efficient endosome-to-Golgi transport of Shiga toxin is dependent on dynamin and clathrin. J Cell Sci 117: 2321–2331.

6. Mayor S, Pagano RE (2007) Pathways of clathrin-independent endocytosis. Nat Rev Mol Cell Biol 8: 603–612.

7. Nicholsa BJ, Kenworthya AK, Polishchuka RS, Lodgea R, Robertsa TH, et al. (2001) Rapid cycling of lipid raft markers between the cell surface and Golgi complex. J Cell Biol 153: 529–541.

8. Saint-Pol A, Yélamos B, Amessou M, Mills IG, Dugast M, et al. (2004) Clathrin adaptor epsinR is required for retrograde sorting on early endosomal membranes. Dev Cell 6: 525–538.

9. Römer W, Berland L, Chambon V, Gaus K, Windschiegl B, et al. (2007) Shiga toxin induces tubular membrane invaginations for its uptake into cells. Nature 450: 670–675.

10. Sens P, Johannes L, Bassereau P (2008) Biophysical approaches to protein-induced membrane deformations in trafficking. Curr Opin Cell Biol 20: 476–482.

11. Reynwar BJ, Illya G, Harmandaris VA, Müller MM, Kremer K, et al. (2007) Aggregation and vesiculation of membrane proteins by curvature-mediated interactions. Nature 447: 461–464.

12. Bast DJ, Banerjee L, Clark C, Read RJ, Brunton JL (1999) The identification of three biologically relevant globotriaosyl ceramide receptor binding sites of the Verotoxin 1 B subunit. Mol Microbiol 32: 953–960.

13. Binder WH, Barragan V, Menger FM (2003) Domains and rafts in lipid membranes. Angew Chem Int Ed 42: 5802–5827.

14. Meder D, Simons K (2006) In: Fielding CJ, ed. Lipid Rafts and Caveolae. Weinheim: WILEY-VCH. pp 1–22.

15. Nyholm PG, Magnusson G, Zheng Z, Norel R, Binnington-Boyd B, et al. (1996) Two distinct binding sites for globotriaosyl ceramide on verotoxins: identification by molecular modelling and confirmation using deoxy analogues and a new glycolipid receptor for all verotoxins. Chem Biol 3: 263–275.

16. Arab S, Lingwood CA (1996) Influence of phospholipid chain length on verotoxin/globotriaosyl ceramide binding in model membranes: comparison of a supported bilayer film and lipoosomes. Glycoconjugate J 13: 159–166.

17. Boyd B, Magnusson G, Zhiuyan Z, Lingwood CA (1994) Lipid modulation of glycolipid receptor function. Availability of Gal(α1–4)Gal disaccharide for verotoxin binding in natural and synthetic glycolipids. Eur J Biochem 223: 873–878.

18. Pellizzari A, Pang H, Lingwood CA (1994) Binding of verocytotoxin 1 to its receptor is influenced by differences in receptor fatty acid content. Biochemistry 31: 1363–1370.

19. Bacia K, Scherfeld D, Kahya N, Schwille P (2004) Fluorescence correlation spectroscopy relates rafts in model and native membranes. Biophys J 87: 1034–1043.

20. Baumgart T, Hess ST, Webb WW (2003) Imaging coexisting fluid domains in biomembrane models coupling curvature and line tension. Nature 425: 821–824.

21. Chiantia S, Kahya N, Ries J, Schwille P (2006) Effects of ceramide on liquid-ordered domains investigated by simultaneous AFM and FCS. Biophys J 90: 4500–4508.

22. Saslowsky DE, Lawrence J, Ren X, Brown DA, Henderson RM, et al. (2002) Placental alkaline phosphatase is efficiently targeted to rafts in supported lipid bilayers. J Biol Chem 277: 26966–26970.

23. Milhiet PE, Giocondi MC, Le Grimellec C (2002) Cholesterol is not crucial for the existence of microdomains in kidney brush-border membrane models. J Biol Chem 277: 875–878.

24. Rinia HA, de Kruijff B (2001) Imaging domains in model membranes with atomic force microscopy. FEBS Lett 504: 194–199.

25. Rinia HA, Snel MM, van der Eerden JP, de Kruijff B (2001) Visualizing detergent resistant domains in model membranes with atomic force microscopy. FEBS Lett 501: 92–96.

26. Dietrich C, Bagatolli LA, Volovyk ZN, Thompson NL, Levi M, et al. (2001) Lipid rafts reconstituted in model membranes. Biophys J 80: 1417–1428.

27. Dietrich C, Volovyk ZN, Levi M, Thompson NL, Jacobson K (2001) Partitioning of Thy-1, G_{M1}, and cross-linked phospholipid analogs into lipid rafts reconstituted in supported model membrane monolayers. Proc Natl Acad Sci USA 98: 10642–10647.

28. Falguières T, Römer W, Amessou M, Afonso C, Wolf C, et al. (2006) Functionally different pools of Shiga toxin receptor, globotriaosyl ceramide, in HeLa cells. FEBS J 273: 5205–5218.

29. Wang R, Shi J, Parikh A, Shreve A, Chen L, et al. (2004) Evidence for cholera aggregation on G_{M1}-decorated lipid bilayers. Colloids Surf B Biointerfaces 33: 45–51.

30. Fraser ME, Chernaia MM, Kozlov YV, James MNG (1994) Crystal structure of the holotoxin from Shigella dysenteriae at 2.5 Å resolution. Nature Struct Biol 1: 59–64.

31. Stein PE, Boodhoo A, Tyrrell GJ, Brunton JL, Read RJ (1992) Crystal structure of the cell-binding B oligomer of verotoxin-1 from E. coli. Nature 355: 748–750.

32. Menke M, Gerke V, Steinem C (2005) Phosphatidylserine membrane domain clustering induced by annexin A2/S100A10 heterotetramer. Biochemistry 44: 15296–15303.

33. Veatch SL, Keller SL (2005) Seeing spots: complex phase behavior in simple membranes. Biochim Biophys Acta 1746: 172–185.

34. Menke M, Künneke S, Janshoff A (2002) Lateral organization of G_{M1} in phase-separated monolayers visualized by scanning force microscopy. Eur Biophys J 31: 317–322.

35. Baumgart T, Hunt G, Farkas ER, Webb WW, Feigenson GW (2007) Fluorescence probe partitioning between Lo/Ld phases in lipid membranes. Biochim Biophys Acta 1768: 2182–2194.

36. Garcia-Saéz AJ, Chiantia S, Schwille P (2007) Effect of line tension on the lateral organization of lipid membranes. J Biol Chem 282: 33537–33544.

37. Lipowsky R (2002) Domains and rafts in membranes - hidden dimensions of self organization. J Biol Phys 28: 195–210.

38. Sens P, Safran SA (2000) Inclusions induced phase separation in mixed lipid films. Eur Phys J E 1: 237–248.

39. Johannes L, Tenza D, Antony C, Goud B (1997) Retrograde transport of KDEL-bearing B-fragment of Shiga toxin. J Biol Chem 272: 19554–19561.

40. Mathivet L, Cribier S, Devaux PF (1996) Shape change and physical properties of giant phospholipid vesicles prepared in the presence of an AC electric field. Biophys J 70: 1112–1121.